RAPID HPHT ANNEALING OF SYNTHETIC IB-TYPE DIAMONDS

V.N. Kazuchits[1], N.M. Kazuchits[1], M.S. Rusetskiy[1], O.V. Korolik[1], A.V. Konovalova[2], O.V. Ignatenko[2*]

[1]*Belarusian State University, Minsk, 220004 Independence Ave. 4*
[2]*State Scientific and Production Association «Scientific and Practical Material Research Center of the NAS of Belarus», 220072, Minsk, P. Brovki str., 19.*
[*]*Corresponding author E-mail address: Ignatenkoov@yahoo.com (O.V. Ignatenko).*

Abstract

The paper provides the information on the effects of rapid (1 minute) high pressure high temperature (RHPHT) annealing of synthetic Ib-type diamond plates at temperatures (1900 °C, 2100 °C, 2300 °C, 2500 °C, 2700 °C) and pressure of 8 GPa. The studies were carried out using the visual analysis, absorption and Raman spectroscopy, photoluminescence and cathodoluminescence. During RHPHT annealing the diamond plates in a high-pressure container were rapidly heated/cooled at a very non-uniform temperature and pressure distribution. All this caused the inhomogeneous plastic deformation of diamond plates. The plastic deformation of diamonds during RHPHT annealing was a powerful "generator" of vacancies. The electron transfer from individual atoms of substituting nitrogen to nitrogen-vacancy centers switched these centers to a negatively charged state. Another accompanying RHPHT annealing process was the diffusion of nitrogen atoms with the formation of it's simple aggregates – H3 defects (at 2300°C). At higher RHPHT annealing temperatures more complex aggregates containing three nitrogen atoms – N3 defects — were generated. RHPHT annealing led to the formation of identical nitrogen – vacancy defects, as did quasi stationary HPHT annealing, but the number of these defects was significantly greater after RHPHT annealing.

Introduction

The heat treatment (annealing) is a common method of controlling diamond properties. Since a diamond at normal pressure is a metastable phase of carbon, it undergoes spontaneous graphitization when heated. Conventionally, the low-temperature annealing in which intrinsic interstitials, vacancies, and hydrogen become movable, can be carried out at normal pressure and without graphitization in the nitrogen or inert gas atmosphere. The generation of color centers in irradiated diamonds [1-3] or the hydrogen diffusion [4] are common examples of such annealing. Modern advances in diamonds annealing technology without pressure allow it to be carried out at high temperatures (low pressure high temperature - LPHT annealing) when impurity nitrogen atoms become mobile [5-9]. The graphitization by LPHT annealing in pure hydrogen atmosphere [7, 10] or in vacuum [11] is significantly suppressed. It is impossible to completely get rid of graphitization despite the significant success of LPHT annealing technology.

To minimize the graphitization the high-temperature diamond annealing is preferably carried out under a pressure stabilizing the diamond phase. The high pressure high temperature (HPHT) annealing in diamond synthesis plants is a typical example of such treatment [12]. The pressure and temperature ranges at HPHT annealing is 5-7 GPa and 1800-2500° C, respectively. The time for temperature setting in BARS-type devices [13-14] designed for the synthesis of large diamond crystals is about 60 minutes, the annealing duration is from a few minutes to several hours, the cooling time to 600-500°C is about 20 minutes. The structural and impurity transformations in synthetic diamonds during HPHT annealing go towards the generation of material similar to natural diamonds. With the account of all advantages of such HPHT annealing, its practical implementation requires expensive equipment and qualified maintenance personnel.

At the same time, HPHT annealing can be performed at a lower cost in high-pressure devices designed for the synthesis of diamond powders [15]. The duration of the heat treatment in the powder synthesis apparatus is comparable to the heating time to a high temperature and is tens of seconds. Using the terminology from silicon-based microelectronics technology we called this treatment rapid high pressure high temperature (RHPHT) annealing. Although the effect of such annealing on diamonds has hardly been studied, it is clear that the samples to be heated will be under very non-equilibrium conditions.

The research results for the defective conversions in RHPHT-treated synthetic Ib-type HPHT diamonds are given below.

Sample preparation and annealing

The plates made of single crystals of Ib-type diamond synthesized at AdamasInvest LLC, Belarus (Almazot trademark) were subjected to rapid thermal annealing. Diamonds were synthesized by the temperature gradient method in C-Fe-Ni melt at temperatures 1470-1500°C and pressure 5.4-5.0 GPa within 70-76 hours [16-17]. The experimental plates were cut along the plane (100) parallel to the base from three crystals grown under the same conditions. A photograph of one of the crystals weighing 1.6 carats is shown in Figure 1. Dashed lines in Figure 1 show the region of the crystal from which the plates were cut. The thickness of the plates was 350-500 μm after the double-sided mechanical polishing. Five rectangular plates with a diagonal size not more than 5 mm were selected for the experiment. The size limitation of the plates was set by the annealing container diameter.
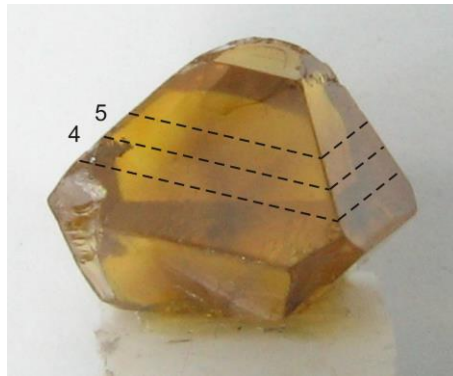
Figure 1 – Photograph of a standard Almazot crystal; experimental plates were cut from the part of the crystal indicated by dashed lines

The diamond plates prepared in this way were annealed at SSPA SPMRC of NAS of Belarus in high-pressure apparatuses with toroid carbide matrices. This type of apparatus is commonly used for the synthesis of diamond and boron nitride micropowders [15]. A high pressure lithographic container with a diamond plate therein was installed in the carbide matrix. Figure 2 shows the arrangement of the diamond plate (1) in the center of the container (2) of the operating volume 222 mm^3 and a diameter 5.8 mm. A fine boron nitride powder (3) with a grain size less than 10 μm was used to create a quasi-hydrostatic pressure distribution in the working volume of the container. The pressure calibration was carried out at the room temperature by phase transitions of solid solutions of zinc and cadmium sulphides and selenides CdS (2.4 GPa), $Zn_{0.05}Cd_{0.95}S$ (3.5 GPa), $Zn_{0.05}Cd_{0.95}S$ (5.3 GPa), CdSe (2.5 GPa), $Zn_{0.07}Cd_{0.93}Se$ (3.3 GPa), $Zn_{0.13}Cd_{0.87}Se$ (4.1 GPa), $Zn_{0.2}Cd_{0.8}Se$ (4.6 GPa), $Zn_{0.3}Cd_{0.7}Se$ (5.6 GPa). Temperature calibration was carried out at a pressure of 8 GPa using a platinum-platinum-rhodium (Pt-Pt / 10% Rh) thermocouple, a graphite-diamond (2600 °C) phase transition, and by the melting points of molybdenum (2700 °C) and iron (1800 °C). The container was heated by electric current passing through cylindrical graphite heater (4) simultaneously with the load application. Diamond plates were annealed at different temperatures (1900°C, 2100°C, 2300°C, 2500°C, 2700°C) and the same pressure - 8 GPa for a minute.
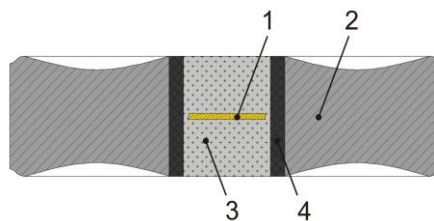
1 – diamond plate;
2 – lithographic stone container casing;
3 – pressure transmitting medium (boron nitride powder);
4 – cylindrical graphite heater.

Figure 2 – Layout of the diamond plate in a high-pressure container at RHPHT annealing

The time of heating to the preset temperature was 60 seconds. On the annealing completion, the pressure was maintained for a cell cooling to the room temperature, which was about 60 seconds.

Research methods

A 12^x magnification optical microscope was used for the visual analysis and photographing of diamond plates. The plates were photographed on a white background lighted by daylight and ultraviolet (UV) light from a 337-nm laser on a black non-luminescent background. The photographing on a black background lighted by UV light of the plates allowed the visualization of photoluminescence (PL) centers distribution. The birefringence photos were taken in transmitted white light when diamond plates were placed between two crossed polarizers.

The ultraviolet-visible (UV) absorption was measured using a Cary 300 Bio dispersion spectrometer. The measurements were carried out at room temperature in a wavelength range of 200-900 nm with a pitch of 0.2 nm. The diameter of the diaphragm limiting the measurement area was 0.8 mm.

The absorption of samples in the visible and near infrared (IR) regions of the spectrum cooled to a temperature of T = 80 K was measured by a laboratory apparatus with a spectral resolution of 0.4 nm. The light passed through the sample was recorded by a silicon photodetector. The spectral range of measurements was 360-1000 nm. The diameter of the area-limiting diaphragm was 0.8 mm.

The absorption in IR spectrum range was recorded by Vertex 70 Fourier-transform IR spectrometer. The measurements were carried out at room temperature with a resolution of 0.5 cm^{-1} in the wave number range from 400 to 4000 cm^{-1} and an average of 60 independent spectrum scans. The diaphragm 1.1 mm in diameter limiting the measurement area was placed directly on the sample surface. The absorption spectra normalization was carried out related to the intrinsic absorption of the diamond lattice, which was (4.6 ± 0.3) cm^{-1} at 2560 and 2430 cm^{-1} or (12.8 ± 0.3) cm^{-1} at 2030 and 1970 cm^{-1} [18]. The absorption coefficients of the main nitrogen centers were detected by decomposing of the measured spectra into three components associated with the absorption by C-defects (single substituting nitrogen atoms in a neutral charge state), N$^+$-defects (positively charged single substituting nitrogen atoms) and A-defects (nearest adjacent pairs of nitrogen atoms in diamond lattice nodes).

The concentration of C-defects was calculated by the absorption at 1130 cm^{-1} using the ratio [19]:

$$N_C \text{ [ppm]} = 25 \cdot \alpha_{1130} \text{ [cm}^{-1}]$$ (1),

where α_{1130} is the absorption coefficient at 1130 cm^{-1}.

The concentration of N$^+$-defects associated with absorption at 1332 cm^{-1} was calculated by formula from [20]:

$$N_{N^+} \text{ [ppm]} = 5.5 \cdot \alpha_{1332} \text{ [cm}^{-1}]$$ (2),

where α_{1332} is the absorption coefficient at 1332 cm^{-1}.

The concentration of A-defects was calculated according to the absorption at a wave number of 1280 cm^{-1} [21]:

$$N_A \text{ [ppm]} = 16.5 \cdot \alpha_{1280} \text{ [cm}^{-1}]$$ (3),

where α_{1280} is the absorption coefficient at 1280 cm^{-1}.

Raman and PL spectra were measured at the room temperature using a NanoFinder High End spectrometer (LOTIS TII Tokyo Instruments) combined with a three-dimensional scanning confocal microscope. Solid state lasers with a wavelength of 355 nm, 473 nm, 532 nm, and 785 nm were used for excitation. The laser radiation was focused on the surface of the samples with a 100^x objective to the spot about 1 μm in diameter. The power of exciting Raman laser radiation varied from 60 μW to 20 mW. Raman spectra were recorded according to the backscattering

pattern of a silicon CCD matrix cooled to -59°C. The spectral resolution was about 0.25 cm^{-1} when the main Raman line was recorded with a high resolution. The general Raman/PL spectra were recorded with a resolution of no less than 3 cm^{-1}. The signal accumulation time ranged from 1 to 120 s.
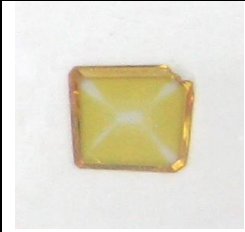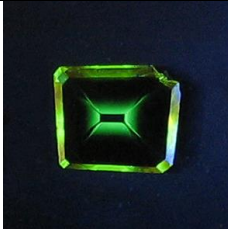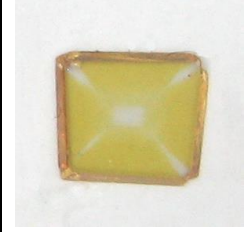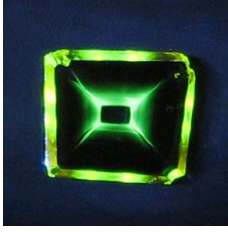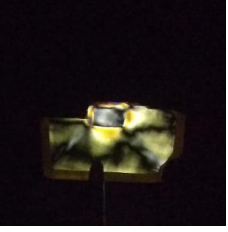
The measurements of cathodoluminescence (CL) spectra of liquid nitrogen cooled samples were carried out using a laboratory device with a spectral resolution of 0.2 nm and a photomultiplier as a photodetector [22]. The spectral range of measurements was 360-900 nm. The luminescence was excited by an electron beam focused on the sample surface to a spot about 1 mm in diameter. All measurements were performed under the same excitation and recording conditions.

Results and discussion

Visual analysis

Table 1 shows photographs of Almazot plates before and after annealing. Annealed plates were etched for 5 minutes in a potassium dichromate boiling solution in sulfuric acid before photographing to remove the surface graphitized layer. As shown in photographs given in Table 1 the original Almazot plates are non-uniformly colored in yellow. The cubic growth sectors that are clearly seen in the central part of plates No. 4102-5, No. 4102-4, and No. 2669-5 are almost colorless or colored in light yellow. The octahedral growth sectors at the plate periphery are colored in yellow. The yellow intensity of synthetic HPHT Ib-type diamonds is determined generally by t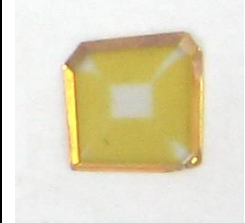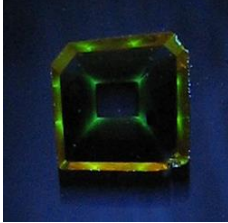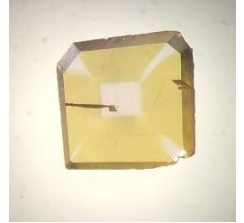he C-defect absorption value [1, 23–25]. The darker yellow corresponds to a higher concentration of C-defects. The standard concentration of C defects in yellow Almazot diamonds is 100–200 ppm [17].

Table 1 Photos of Almazot plates before and after RHPHT annealing

Plate No., annealing temperature	before RHPHT annealing		after RHPHT annealing	
	daylight	UV lighting	daylight	birefringence
4102-5, **1900°C**				
4102-4, **2100°C**				
2669-5, **2300°C**				

4094-5, **2500°C**				
4094-4, **2700°C**				
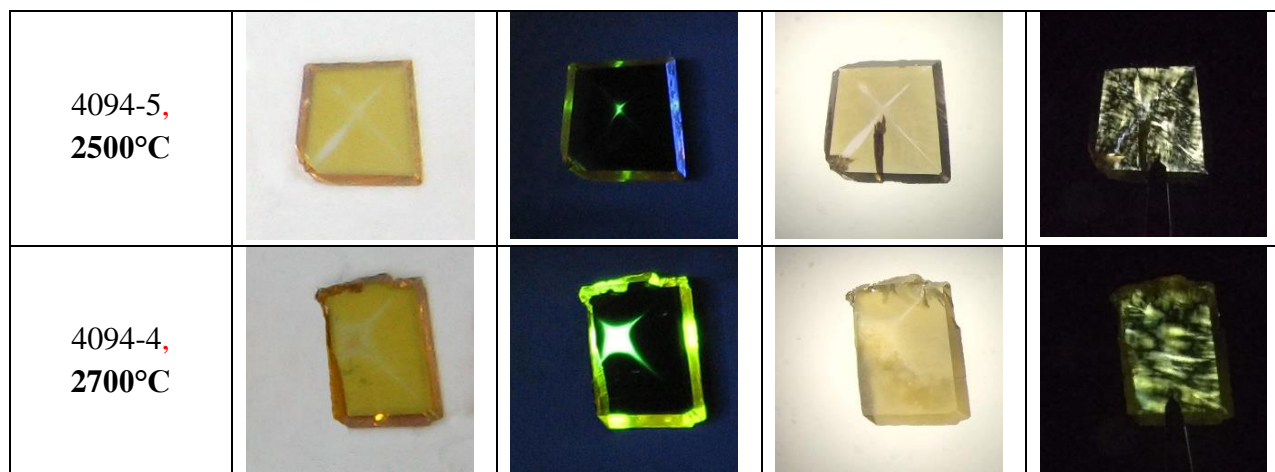
The green PL related to Ni-containing defects [10, 25–30] was observed in the central part of the plates under ultraviolet illumination. The green PL is localized in octahedral growth sectors bordering the cubic sector in the central part of plates No. 4102-5, No. 4102-4, and No. 2669-5. The cubic growth sector was either absent or had a small size in plates No. 4094-5 and No. 4094-4. The green PL in these plates is mainly localized near the edges of the octahedral growth sectors. PL had the maximum intensity at the edge between growth sectors in all plates. PL intensity abruptly disappeared in the cubic growth sectors, while it gradually declined in the octahedral sectors. Such distribution of PL intensity reflected effective nickel capture by intersector edges and octahedral growth sectors and the low efficiency of nickel capture by cubic sectors during synthesis [10, 28–29].

The color of the cubic growth sectors practically did not change, and the octahedral sectors became light yellow after RHPHT annealing. The edge between the cubic and octahedral sectors was marked more clearly. The surface of plates annealed at temperatures above 2300°C became matte greatly diffusing the visible light. The cracks occurred in plates No. 2669-5 and No. 4094-5 annealed at 2300°C and 2500°C, respectively, and plate No. 4102-4 collapsed. The cracks were formed in plane (110) and did not spread further than the middle of the plates. Thus, the relative shift of different parts of the plates during RHPHT annealing was insignificant. The destruction of plate No. 4102-4 was mainly caused by its large size and possible contact with the walls of the high pressure container during RHPHT annealing. Note the significant surface graphitization of plate No. 4094-4 after annealing at 2700°C. It seems that the pressure generated by the plant during RHPHT annealing at 2700°C was insufficient to stabilize the diamond phase.

The green PL region a little spread to the octahedral growth sectors (the corresponding photographs are not shown in Table 1) after RHPHT annealing and occupied a large area. The spread of green PL was related to the generation of additional nickel-containing centers during annealing [10]. The green PL was absent in cubic growth sectors, as before RHPHT annealing.

The cross-polarization microscopy was used to reveal stresses. The dark field condition was achieved by two cross-polarizers. The deviation from the dark field condition arising due to the birefringence gave the optical contrast. Due to the varying of birefringence with stress, we could identify its distribution. The photographs in Table 1 in "crossed polarizers" made it possible to visualize the stress distribution in diamond plates after RHPHT annealing. The birefringence was not observed before RHPHT annealing and at annealing temperatures not higher than 1900°C (see photo of plate No. 4102-5). As can be seen from the photo of plate No. 4102-4, the stressed areas appeared after RHPHT annealing at 2100°C as large bright spots near

the edge of the cubic and octahedral growth sectors. The intensity of the transmitted light indicated that the stress amount in this plate decreased towards the periphery of the octahedral sectors. The pattern of stress distribution at higher temperatures was formed by alternating light and dark stripes directed from the center of the plate to its periphery (see photo No. 2669-5 and No. 4094-5). The increase of RHPHT annealing temperature to 2300°C and 2500°C was accompanied by the reduction of the stress strips size with the simultaneous increase of their quantity per area unit. The size of the stressed strips increased and their density decreased after the maximum temperature of RHPHT annealing (see photo No. 4094-4).

The birefringence in diamonds was observed after the plastic deformation caused by the graphitization during the elastic deformation near inclusions, dislocations, grain edges, and edges of growth sectors [31–34]. The possible cause of stress generation in our case was the plastic deformation of the plates during RHPHT annealing. It is obvious that the pressure was not hydrostatic, but was heterogeneously distributed during RHPHT annealing. This is evidenced by the cracks in the plates appeared after the annealing at temperatures of 2300°C and 2500°C. The inhomogeneous pressure distribution during RHPHT annealing caused the plastic deformation and stress in the plates manifested in the birefringence pattern and in the spectral shift of the CRC main line.

Raman scattering

Figure 3a (using the example of plate No. 2669-5) shows standard Raman spectra of Almazot from cubic and octahedral growth sectors before RHPHT annealing. The spectra were measured at room temperature. The spectra contained a very intense narrow line (R) at 1332 cm^{-1} of the single-phonon light scattering in diamond and pronounced double-phonon scattering band (R2) in the range of 2200 to 2660 cm^{-1} before RHPHT annealing. There were no signs of graphite phase in the Raman spectra [35]. The spectrum from the octahedral sector contained a line at 800 cm^{-1} (491 nm) that is most likely related to luminescence. The spectral position of the Raman main line was at 1332.15 cm^{-1} before RHPHT annealing. Its full width at half maximum (FWHM) was 1.63 cm^{-1} in the cubic growth sector with about 10 ppm of the nitrogen concentration and 1.75 cm^{-1} in the octahedral sectors with about 180 ppm of the nitrogen concentration. The Raman main line width in structurally perfect nitrogen-free IIa-type diamonds was about 1.6 cm^{-1} [36–39]. Therefore, the pre-annealing expansion of line 1332 cm^{-1} with respect to IIa-type diamonds for plate No. 2669-5 was related to the higher nitrogen concentration, as [37, 39].
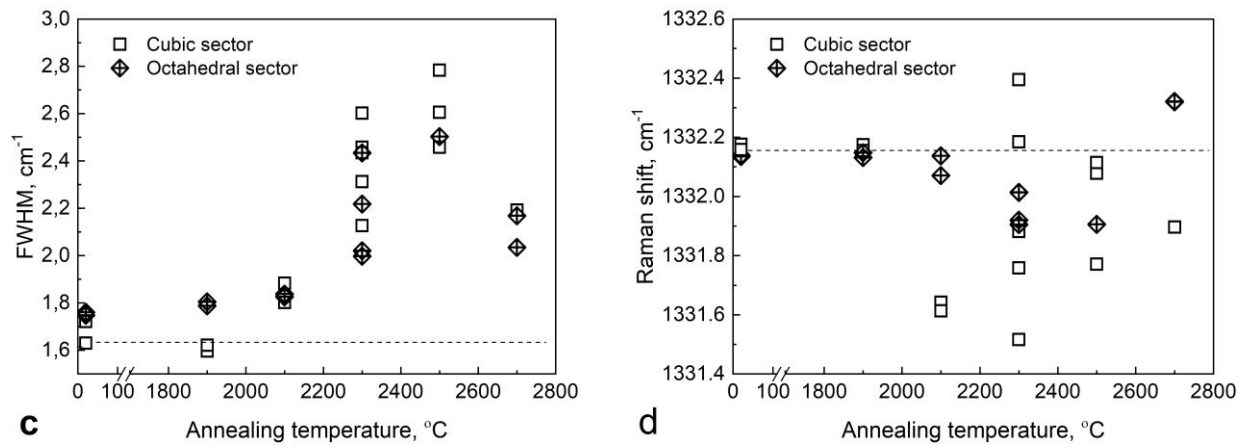

a

b
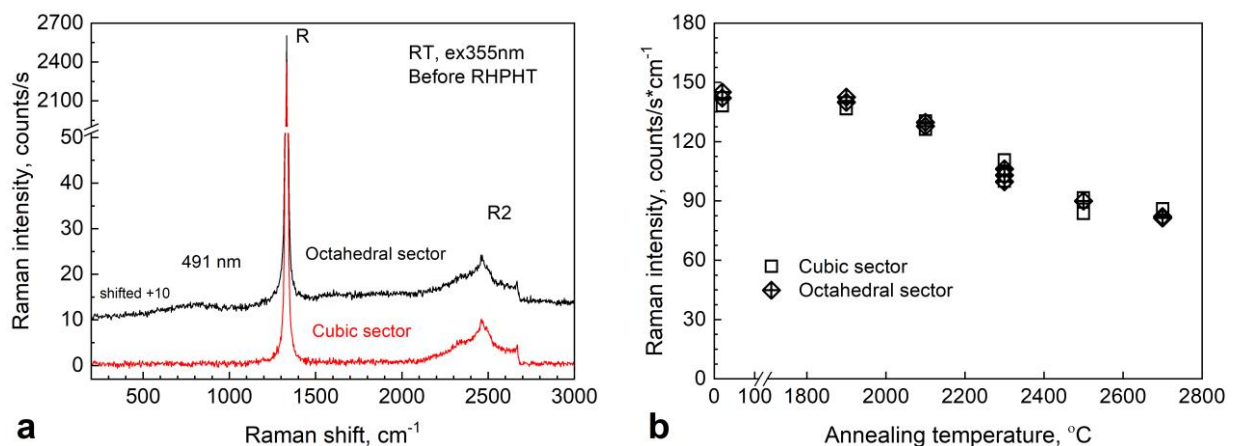
Figure 3 – Raman spectra of Almazot (a) from the cubic and octahedral sectors before RHPHT annealing, (b) integral intensity; (c) FWHM, and (d) the spectral position of 1332 cm⁻¹ line vs. temperature RHPHT annealing. The dashed line shows the parameters of 1332 cm⁻¹ line in nitrogen-free areas of the plates before RHPHT annealing

The Raman intensity decreased and intense PL appeared after RHPHT annealing. The laser excitation with a wavelength of 785 nm was used to suppress PL.

Figures 3b, 3c, 3d show the changes in the Raman main line parameters after RHPHT annealing. Raman spectra were recorded at the excitation of randomly selected areas on the surface of plates in cubic and octahedral growth sectors. As you can see, 1332 cm⁻¹ line widened and in most cases shifted to smaller wave numbers, its integral intensity decreased monotonically with the increase in RHPHT annealing temperature. The significant variation in the spectral position and 1332 cm⁻¹ line width within the plate was observed in both cubic and octahedral growth sectors.

The shift and broadening of the main Raman scattering line was caused by the plastic deformation of diamond during RHPHT annealing and the stresses related to the deformation. As can be seen from the birefringence photographs in Table 1, the diamond plates were locally stressed after RHPHT annealing. The density of the stressed regions in the plates increased with increase of RHPHT annealing temperature. The shift in the spectral position of the main Raman scattering line of diamonds is linearly related to elastic stresses [40–43]. The shift to lower values of the wave number corresponded to the expansion of the diamond crystal lattice, while the shift to the higher wave numbers corresponded to its compression. We estimated the value of elastic stresses σ in direction <001> using the expression given in [43]:

$$\sigma = 0.49 \cdot [\text{GPa} / \text{cm}^{-1}] \cdot \Delta\nu \, [\text{cm}^{-1}] \tag{4},$$

where $\Delta\nu$ is the difference between the spectral position of 1332 cm⁻¹ line before and after RHPHT annealing. Taking into account the above expression, the elastic stress value between the most compressed and stretched regions of the plate was about 0.43 GPa after RHPHT annealing at a temperature of 2.300°C.

Absorption

Visible-near IR range

The absorption spectra of Almazot octahedral growth sectors in the visible spectral range are shown in Figure 4. Almazot plates absorbed intensively the radiation with wavelengths less

than 500 nm. Such absorption shown as an example in Fig. 4a is typical for synthetic HPHT diamonds containing C-defects and determined their yellow color [1, 13, 23–24]. The absorption maximum of C-defects was at 270 nm [2, 23]. The samples were almost non-transparent at the absorption maximum, and the spectra contained only the long wavelength absorption edge of C-defects starting from 500 nm [13] at C-defects concentration more than 50 ppm.
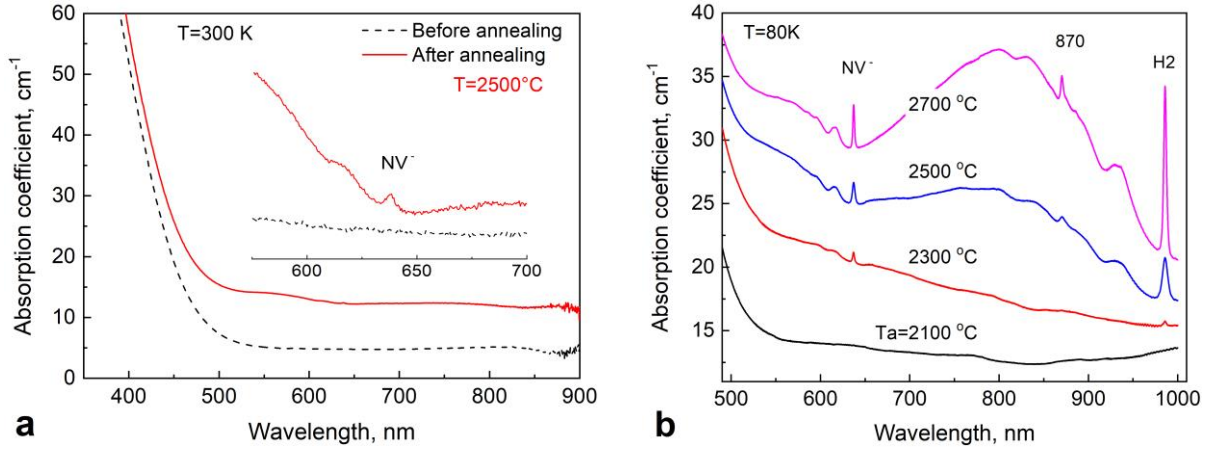

Figure 4 – Absorption spectra of octahedral growth sectors in Almazot plates: a) – at room temperature before and after RHPHT annealing at T = 2500°C, b) – at liquid nitrogen temperature after RHPHT annealing. The inset in Fig. 4a shows a part of the spectrum in the vicinity of the NV⁻-center

The surface of the diamond plates became matte and the absorption spectra shifted along the ordinate axis to larger values by approximately 4–7 cm^{-1} due to light scattering after RHPHT annealing (see Fig. 4a). The line at 638 nm appeared at the spectra of absorption by octahedral growth sectors starting from 2100°C temperature (see the inset in Fig. 4a). The absorption at 638 nm in cubic growth sectors and in the central luminescent areas of the plates was practically absent. Such distribution of 638 nm centers is typical for synthetic HPHT Ib-type diamonds [44] in which they were formed mainly in (111) growth sectors and were almost absent in (100) sectors.

638 nm center (NV⁻-center) was related to the nitrogen-vacancy complex in the negative charge state [45]. This center is typical for all nitrogen-containing diamonds, especially intense in Ib-type diamonds where the C-form of nitrogen prevails. NV⁻-center in Ib-type diamonds is formed after any type of irradiation and subsequent annealing at vacancy migration temperatures (46–47). The formation of NV⁻-centers was also observed after the plastic deformation of diamonds and high-temperature annealing under pressure [48]. The ratio [20] between concentrations (cm^{-3}) of 638 nm centers and the integrated absorption of their respective zero-phonon lines (in meV cm^{-1}) for measurements at 80 K is determined as follows:

$$N_{NV^-}\ [cm^{-3}] = 8.9 \cdot 10^{15} \cdot I_{638}\ [meV \cdot cm^{-1}] \tag{5},$$

where I_{638} is the area under NV⁻-center line in the absorption spectra presented in units of [meV·cm^{-1}].

The transformation of the absorption spectra with increase of RHPHT annealing temperature of diamond plates is shown in Figure 4b. To obtain more distinct structure of the spectra and to extract the concentration of NV⁻-centers the diamond plates were cooled to the temperature of liquid nitrogen during absorption measurements. As can be seen from Figure 4b

additional absorption lines appeared at 870 nm and 986 nm in the spectra along with the line of 638 nm after RHPHT annealing at 2300°C. The width, integrated intensity of 638 nm, 870 nm, 986 nm lines, and the concentration of NV⁻-centers calculated using expression (5) are shown in Table 2. The intensity of all lines increased due to RHPHT annealing temperature.

Table 2 – Some characteristics of absorption by defective centers after RHPHT annealing

RHPHT annealing temperature, °C	FWHM, meV / integrated intensity, meV·cm^{-1} / concentration, cm^{-3}		
	638 nm (NV⁻)	870 nm	986 nm (H2)
1900	-	-	-
2100	5.80 / 0.20 / **1.76e15**	-	-
2300	7.67 / 6.21 / **5.47e16**	6.87 / 0.39	4.90 / 1.67
2500	10.39 / 17.39 / **1.53e17**	8.68 / 4.39	8.92 / 29.44
2700	6.90 / 23.90 / **2.10e17**	4.76 / 8.38	4.88 / 65.14

The 986 nm center (H2 center) is an A-defect that has captured the vacancy in the negative charge state forming a structure of (NVN)⁻ type - a pair of substituting nitrogen atoms separated by a negatively charged vacancy [45, 49, 50]. A negative vacancy charge is obtained by capturing a weakly bound electron from closely spaced nitrogen atoms in the C-form [2, 49, 51]. The line at 870 nm is generated due to the interaction of H2-center with its own local vibrations with the energy of about 167 meV according to [50]. The formation of H2-centers is the firm evidence of the nitrogen aggregation during RHPHT annealing. The increase in the absorption intensity at 986 nm simultaneously with the increase in RHPHT annealing temperature indicates the increase in the aggregated nitrogen concentration.

It should be noted that absorption spectroscopy methods did not reveal nitrogen-vacancy centers in the neutral charge state after RHPHT annealing, such as H3 at 503 nm (NVN)⁰ and at 575 nm (NV⁰). This is possible if the concentration of C-defects significantly exceeds the concentration of all nitrogen-vacancy centers corresponding to our case. In fact, the usual concentration of C-defects in Almazot yellow crystals was about 100-200 ppm [7, 16, 17] and the concentration of NV-centers, for example, was about 1 ppm (see Table 2).

IR range

Figure 5 shows the absorption spectra in the IR spectral range before and after RHPHT annealing, for example, at a temperature of 2700°C. The measurements were carried out in the central part of the plate (Figure 5a) and on the periphery of the plate in the octahedral growth sector (Figure 5b). The similar measurements were performed for all plates.
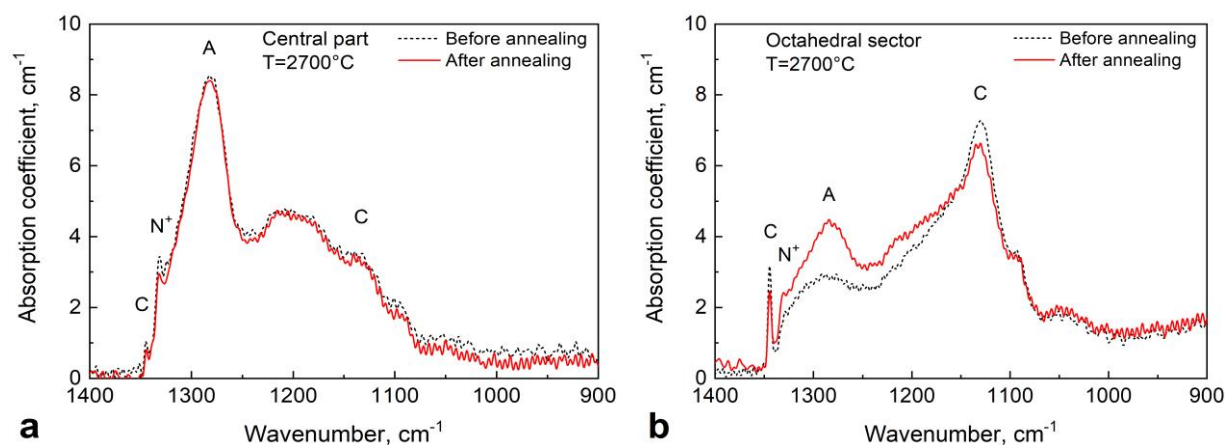
Figure 5 – Absorption spectra in the IR spectral range before and after RHPHT annealing: a) – in the central part of the plate, b) – the octahedral growth sector at the periphery of the plate

The structure of the IR absorption spectra in the central part of the plates before RHPHT annealing was almost the same for all samples. The absorption by the simplest aggregates - the A-form of nitrogen at 1280 cm^{-1}, related to the oscillations of two nearest nitrogen atoms at the diamond lattice nodes, prevailed. The nitrogen concentration in the A-form for the spectrum of sample 4094-4 shown in Figure 5a was about 125 ppm. The absorption of single isolated nitrogen atoms at the lattice nodes (C-form of nitrogen) at 1130 and 1345 cm^{-1} corresponded to a concentration of about 38 ppm. The absorption related to the ionized C-form of nitrogen, N$^{+,}$ was about 10 ppm. As shown in Figure 5a, the absorption spectrum for the central part of the plate practically did not change after RHPHT annealing at 2700°C. The absence of changes was due to the fact that a significant part of nitrogen in the central area of the plates has been already aggregated during the synthesis [7, 10, 29, 52]. The additional short-term RHPHT annealing did not lead to the noticeable additional nitrogen aggregation in these areas even at 2700°C. Only a slight increase in absorption by N$^+$ form of nitrogen can be noted. This increase can be either due to the formation of additional nitrogen-nickel centers or mismatch of the IR probing areas before and after annealing.

In contrast, the spectra from octahedral growth sectors at the plate periphery changed after RHPHT annealing due to the aggregation of nitrogen from C- to A-form [7, 10, 53–55]. The nitrogen concentration calculated from the absorption spectra for the peripheral areas of the plates is shown in Table 3. As shown in Figure 5b, the nitrogen in the octahedral sectors of the plates was mainly in C-form at the concentration of about 169 ppm before RHPHT annealing. The absorption of C-form decreased to 139 ppm after RHPHT annealing at 2700°C. In contrast, the absorption of A-form nitrogen increased from 8 to 36 ppm after RHPHT annealing. The concentration of N$^+$ nitrogen form also increased slightly from 3 to 5 ppm.

Table 3. The approximate nitrogen concentration in the octahedral growth sectors at the periphery of the plates before and after RHPHT annealing

Temperature, °C	Nitrogen concentration before→after RHPHT annealing, ppm (+/- 5%)			
	C-form	N$^+$-form	A-form	**C+N$^+$+A**
1900	121 → 118	8 → 6	35 → 30	164 → 154
2100	115 → 130	9 → 7	36 → 35	160 → 172

2300	173 → 174	2 → 4	9 → 8	184 → 186
2500	167 → 163	3 → 9	4 → 6	174 → 178
2700	169 → 139	3 → 5	8 → 36	180 → 180

As can be seen from Table 3, the detectable nitrogen aggregation in IR absorption was observed at RHPHT annealing temperatures equal to 2500°C and above. The absorption spectra structure did not change practically after RHPHT annealing at lower temperatures. It should be noted that the IR absorption spectra did not contain any features of the second stage of nitrogen aggregation related to the generation of B defects.

Cathodoluminescence

The CL spectra of diamond plates before and after RHPHT annealing are shown in Figure 6. The spectra were recorded during the excitation of octahedral growth sectors. CL spectra structure before RHPHT annealing was typical for synthetic Ib-type diamonds grown from iron-nickel melt [22, 45, 47, 56–58]. The spectra were dominated by the intense zero-phonon line (ZPL) related to the nickel at 484 nm and a wide electron-phonon band with a maximum of about 540 nm. The low-intensity Ni center was also observed - doublet at 884 nm. Both centers had a simple atomic structure and contained one Ni atom according to [59-60].
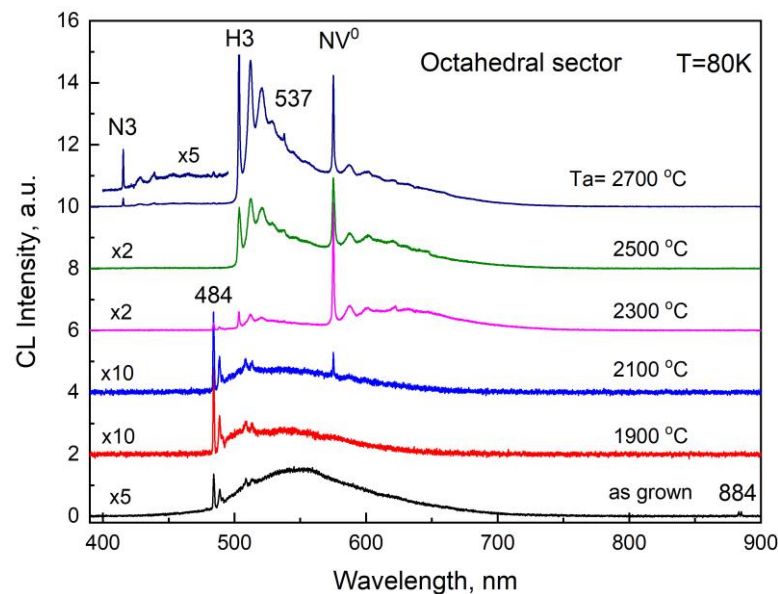
Figure 6 – CL spectra of diamond plates before and after RHPHT annealing recorded during the excitation of the octahedral growth sectors. The spectra are shifted along the ordinate for clarity.

The intensity of the 484 nm center almost did not change after RHPHT annealing at 1900°C – 2100°C. The center at 884 nm was not detected after an annealing temperature of 1900 °C. ZPL at 575 nm appeared in the CL spectra related to the nitrogen-vacancy center in a neutral charging state (NV^0) [45] starting from 2100°C. The formation of NV^0-centers was observed after the plastic diamond deformation and high-temperature annealing under pressure [48, 61]. The intensity of the 484 nm nickel center decreased significantly after annealing at 2300°C. It was no longer dominant. The line at 503 nm appeared in the CL spectra along with the increase

in the intensity of the NV^0-center. The structure of the 503 nm center (H3-center) includes two nitrogen atoms and a vacancy [45]. The registration of the H3-center in the CL spectra indicates the formation of the simplest nitrogen aggregates in the form of two atoms at the nearest adjacent nodes of the diamond lattice. The further increase in the RHPHT annealing temperature to 2500°C caused the annealing of the 484 nm center, the increase in the intensity of the NV^0 and H3-centers, and the appearance of the low intensity line at 537 nm. The 537 nm center in the CL spectra appeared simultaneously with the H3-center [47]. There is an opinion [45] that the 537 nm center is a phonon repetition of 503 nm ZPL arising from the interaction of the electronic transition with 160 meV phonon. The 415 nm line corresponding to the N3-center appeared in the CL spectra at 2700°C. The structure of the N3-center includes 3 nitrogen atoms and a vacancy [45]. The formation of the N3-center after RHPHT annealing at 2700°C indicates the deeper aggregation of nitrogen corresponding to B-form.

Collins and Robertson [62] estimated the internal stresses ratio to the width of the 575 nm zero-phonon line measured at 77 K using the simple expression:

$$\sigma = W_{575} / 10 \cdot \tag{6},$$

where σ is the stress value in GPa and W is FWHM line in meV. The application of this ratio to FWHM values of the 575 nm line extracted from Figure 6 showed that diamond plates contained significant internal stresses varying from about 0.27 GPa to 0.71 GPa after RHPHT annealing at temperatures above 2100°C. This stress values obtained from ZPL width equal to 575 nm are comparable to that obtained from the spectral shift of 1332 cm^{-1} Raman line.

Photoluminescence

The PL spectra of diamond plates shown in Figure 7 were recorded at room temperature after RHPHT annealing and supplemented the results of the CL study. The PL spectra had the same structure and practically did not differ from those shown in Figure 7 for the RHPHT annealing temperature of 1900°C prior to annealing. The spectra contained a wide FL band with a maximum of about 530 nm along with the narrow R and 2R lines from the Raman spectra. The average PL intensity was approximately 10 calculations per second. The subsequent RHPHT annealing at higher temperatures caused the significant increase in PL intensity. 575 nm and 638 nm lines related to nitrogen vacancy centers appeared in the PL spectra starting from 2100°C. The 638 nm line is related to the nitrogen-vacancy center in the negatively charged state [45] that was not excited during CL studies. As shown in Figure 7, 575 nm centers were formed predominantly in the central areas of the plates in the cubic growth sectors, and 638 nm centers were formed on the periphery of the plates in the octahedral sectors [44]. As in CL studies, the 503 nm line appeared in the PL spectra indicating the nitrogen aggregation after RHPHT annealing at 2300°C. Its intensity, as well as the intensity of 575 nm and 638 nm lines, changed with the increase in RHPHT annealing temperature. It should be noted that RHPHT annealing of Almazot in the quasi-stationary mode at the pressure of 5.2 GPa and temperature of 1870°C within 4 hours regularly carried out by the authors (see, for example, [10]) did not cause such intense luminescence.
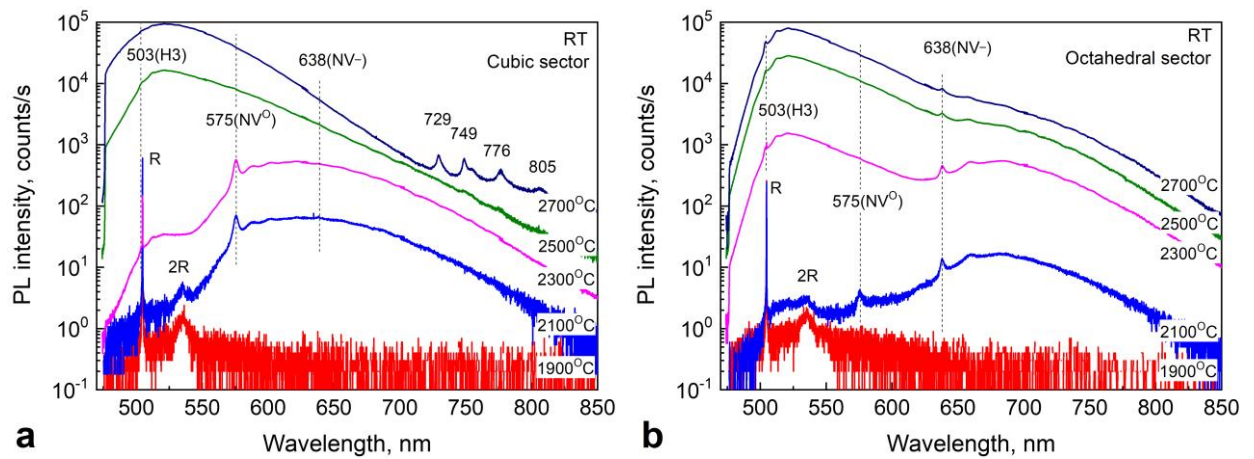
Figure 7 –PL spectra of diamond plates after RHPHT annealing: (a) – in the cubic growth sectors in the central areas of plates, (b) – in the octahedral growth sectors at the periphery of plates; the wavelength of the exciting irradiation is equal to 487 nm

The lines at 729 nm, 749 nm, 776 nm, and 805 nm from the central luminescent area of 4094-4 plate were present in the PL spectra even before annealing. These lines were observed in the PL spectra of synthetic HPHT diamonds grown from nickel-containing carbon solvents [45]. Therefore, their connection with nickel is most likely.

Our observations of changes in Almazot synthetic diamonds after RHPHT annealing correlate with the known information about the formation of nitrogen-vacancy centers in Ib-type diamonds during HPHT annealing. Almazot crystals contained the nitrogen admixture mainly in the C-form after the synthesis. The nitrogen content was higher in octahedral growth sectors than in cubic one. The nitrogen share was in the form of the simplest aggregates - in the A-form in the central part of the crystals near the seed. The aggregated nitrogen fraction in the central part of the crystals depended on the temperature and synthesis duration.

It is known that the high-temperature annealing under pressure caused the plastic deformation of the diamond [63–64] to some extent. The authors of [64–65] observed noticeable manifestations of the plastic deformation at temperatures of 1000°C and higher. The diamond was plastically deformed due to partial graphitization [66] or due to stresses relaxation at the edges of growth sectors [32] even under the hydrostatic pressure distribution during the high-temperature annealing. The plastic deformation was accompanied by the formation of dislocations [48] and the generation of vacancies [67–68].

It is obvious that the rapid heating/cooling of the diamond plates in the high pressure container took place under conditions of a very inhomogeneous temperature and pressure distribution during RHPHT annealing. All this caused the inhomogeneous plastic deformation of the diamond plates. The consequences of the plastic deformation after RHPHT annealing were preserved in the form of stresses "imprinted" in the topogram of the diamond plates birefringence and manifested in the expansion of Raman, absorption, and luminescence lines. As follows from the Raman spectra, the stresses were both compressing and expanding the diamond crystal lattice. The latter prevailed.

The plastic deformation of diamonds during RHPHT annealing was a powerful "generator" of vacancies that participated in the "construction" of nitrogen-vacancy defects. The RHPHT annealed plates could be easily deformed with the increase in temperature, more vacancies were generated, and they were more mobile. The mobile vacancies were captured by

nitrogen atoms and formed nitrogen-vacancy centers. The electron transfer from individual substituting nitrogen atoms to nitrogen-vacancy centers stimulated by the annealing switched some of these centers to the negatively charged state [2, 49, 51].

The distribution of nitrogen vacancy centers in different growth sectors generally corresponded to the distribution of nitrogen impurities. More of them were generated in the octahedral growth sectors with a higher nitrogen concentration during RHPHT annealing. The vast majority of nitrogen-vacancy centers (clearly visible from the absorption spectra) captured electrons from the substituting nitrogen atoms and became negatively charged.

Another process accompanying RHPHT annealing was the diffusion of nitrogen atoms with the generation of its aggregates. The manifestation of the nitrogen aggregation was detected after RHPHT annealing at 2300°C as a result of H2- and H3 defects formation. The concentration of these defects increased at higher RHPHT annealing temperatures, more complex aggregates containing three nitrogen atoms - N3 defects were formed. The sequence of nitrogen-vacancy defects formation with the increase in RHPHT annealing temperature (from simple to more complex) is the same as in quasi-stationary annealing. Qualitatively, RHPHT annealing led to the formation of identical nitrogen-vacancy defects, as well as quasi-stationary HPHT annealing. However, the number of these defects was significantly greater after RHPHT annealing. This difference was due to the higher concentration of vacancies formed under RHPHT annealing.

The difference between RHPHT and quasi-stationary HPHT annealing was that the aggregation was carried out along with the simultaneous generation of a large number of vacancies during RHPHT annealing. It is known that vacancies [6, 55, 69] or interstitial sites [70] created by the preliminary electron irradiation in diamonds accelerated the nitrogen aggregation. Therefore, the expectation of the accelerated nitrogen aggregation in diamonds is fully justified during RHPHT annealing. (The issue of the accelerated nitrogen aggregation in diamonds caused by the plastic deformation of their own defects was not considered in this study.)

The new effect of RHPHT annealing is to increase the luminescence efficiency in diamonds. It can be useful for some practical applications, for example, generation of scintillators [71] and fluorescent markers [9, 72-73].

Conclusions

We perform detailed study of the Ib type diamond plates after rapid annealing in the high-pressure chamber. A part of the results related to the absorption and Raman/luminescence spectroscopy are reported in this communication. Based on these results we made a conclusion that diamond plates were plastic deformed during RHPHT annealing under the influence of non-uniform pressure and temperature distribution. The plastic deformation generated many vacancies, which, being mobile at RHPHT annealing temperatures, formed nitrogen-vacancy defects and accelerated nitrogen aggregation.

Reference

1. A.T. Collins, The colour of diamond and how it may be changed. J. Gemm, 27 №6 (2001) 341-359.

2. A.T. Collins, The detection of colour-enhanced and synthetic gem diamonds by optical spectroscopy. Diamond and related materials, 12 10-11 (2003) 1976-1983.

3. J.E. Shigley, C.M. Breeding, Optical defects in diamond: a quick reference chart, Gems & Gemology 49 2 (2013) 108-111.

4. D.J. Cherniak, E.B. Watson, V. Meunier, N. Kharche, Diffusion of helium, hydrogen and deuterium in diamond: Experiment, theory and geochemical applications, Geochimica et Cosmochimica Acta 232 (2018) 206-224.

5. V.G. Vins, A.P.Yelisseyev, S.S. Lobanov, D.V. Afonin, A.Y. Maksimov, A.Y. Blinkov, APHT treatment of brown type Ia natural diamonds: Dislocation movement or vacancy cluster destruction, Diamond and related materials 19 7-9 (2010) 829-832.

6. A.P. Yelisseyev, V.G. Vins, S.S. Lobanov, D.V. Afonin, A.E. Blinkov, A.Y. Maximov, Aggregation of donor nitrogen in irradiated Ni-containing synthetic diamonds, Journal of crystal growth. 318 1 (2011) 539-544.

7. N.M. Kazuchits, M.S. Rusetsky, V.N. Kazuchits and A.M. Zaitsev, Aggregation of nitrogen in synthetic diamonds annealed at high temperature without stabilizing pressure, Diamond and Related Materials 64 (2016) 202–207.

8. S. Eaton-Magaña, T. Ardon, A.M. Zaitsev, LPHT annealing of brown-to-yellow type Ia diamonds, Diamond and Related Materials 77 (2017) 159-170.

9. L. Dei Cas, S. Zeldin, N. Nunn, M. Torelli, A.I. Shames, A.M. Zaitsev, O. Shenderova, From fancy blue to red: Controlled production of a vibrant color spectrum of fluorescent diamond particles, Advanced Functional Materials 29 19 (2019) 1808362.

10. N.M. Kazuchits, M.S. Rusetsky, V.N. Kazuchits, O.V. Korolik, V. Kumar, K.S. Moe, W. Wang, A.M. Zaitsev, Comparison of HPHT and LPHT annealing of Ib synthetic diamond, Diamond and Related Materials 91 (2019) 156-164.

11. A.M. Zaitsev, B. Deljanin, A. Peretti, M. Alessandri, W. Bieri, New generation of synthetic diamonds reaches the market (part C): Origin of yellow color in CVD-grown diamonds and treatment experiments, Contributions to Gemology 14 (2014) 41-55.

12. I.A. Dobrinets, V.G. Vins, A.M. Zaitsev, HPHT-treated Diamonds: Diamond Forever, Springer Science & Business Media 181 (2013) 257.

13. J.E. Shigley, E. Fritsch, J.I. Koivula, N.V. Sobolev, I.Y. Malinovsky, Y.N. Pal'yanov, The gemological properties of Russian gem-quality synthetic yellow diamonds, Gems & Gemology 29 4 (1993) 228-248.

14. R. Abbaschian, H. Zhu, C. Clarke, High pressure-high temperature growth of diamond crystals using split sphere apparatus, Diamond and related materials 14 11-12 (2005) 1916-1919.

15. A. Olejniczak, R. Tomala, B. Cichy, P. Głuchowski, M. Jakimow, A. Zieba, L. Kepinski, O. Ignatenko, W. Strek, Laser-driven proliferation of sp^2-sp^3 changes during anti-Stokes white light emission of m-diamonds, Carbon 146 (2019) 438-446.

16. A.V. Mudryi, T.P. Larionova, I.A. Shakin, G.A. Gusakov, G.A. Dubrov, V.V. Tikhonov, Optical properties of synthetic diamond single crystals, Semiconductors 38 5 (2004) 520-523.

17. N.M. Kazyuchits, A.V. Konovalova, I.I. Azarko, F.F. Yakotsuk, I.N. Bogdanov, Yu.K. Kabak, Effect of synthesis conditions on the impurity composition of STM "Almazot" diamond single crystals, Inorg. Mater. 50 2 (2014) 130–135.

18. G.B. Bokii, G.N. Bezrukov, Ju.A. Kluev, A.M. Naletov, V.I. Nepsha, Natural and Synthetic Diamonds, Nauka, Moscow, 1986 (in Russian).

19. I. Kiflawi, A.E. Mayer, P.M. Spear, J.A. Van Wyk, G.S. Woods, Infrared absorption by the single nitrogen and A defect centers in diamond, Philos. Mag. B 69 (1994) 1141–1147.

20. S.C. Lawson, D. Fisher, D.C. Hunt, M.E. Newton, On the existence of positively charged single-substitutional nitrogen in diamond, Journal of Physics: Condensed Matter 10 27 (1998) 6171.

21. S.R. Boyd, I. Kiflawi, G.S. Woods, The relationship between infrared absorption and the A defect concentration in diamond, Philos. Mag. B 69 (1994) 1149–1153.

22. N.M. Kazuchits, M.S. Rusetsky, V.N. Kazuchits, A.M. Zaitsev, Cathodoluminescence of synthetic diamonds annealed at high temperature without stabilizing pressure, Diamond and Related Materials. 74 (2017) 41-44.

23. R.C. Burns, V. Cvetkovic, C.N. Dodge, D.J.F. Evans, M.L.T. Rooney, P.M. Spear, C.M. Welbourn, Growth-sector dependence of optical features in large synthetic diamonds, Journal of Crystal Growth 104 2 (1990) 257-279.

24. H. Kanda, Nonuniform distributions of color and luminescence of diamond single crystals, New Diamond and Frontier Carbon Technology 17 2 (2007) 105-116.

25. H. Kanda, K. Watanabe, Distribution of nickel related luminescence centers in HPHT diamond, Diam. Relat. Mater 8 (1999) 1463–1469.

26. A. Yelisseyev, Y. Babich, V. Nadolinny, D. Fisher, B. Feigelson, Spectroscopic study of HPHT synthetic diamonds, as grown at 1500 °C, Diam. Relat. Mater 11 (2002) 22–37.

27. A.P. Yelisseyev, J.W. Steeds, Y.V. Babich, B.N. Feigelson, A new approach to investigation of nickel defect transformation in the HPHT synthetic diamonds using local optical spectroscopy, Diam. Relat. Mater 15 (2006) 1886–1890.

28. I. Kiflawi, H. Kanda, S.C. Lawson, The effect of the growth rate on the concentration of nitrogen and transition metal impurities in HPHT synthetic diamonds, Diam. Relat. Mater 11 (2002) 204–211.

29. Y.V. Babich, B.N. Feigelson, Spatial distribution of the nitrogen defects in synthetic diamond monocrystals: data of IR mapping, Geochemistry International, 47 1 (2009) 94-98.

30. E. Gaubas, T. Ceponis, A. Jasiunas, V. Kalendra, J. Pavlov, N. Kazuchits, E. Naumchik, M. Rusetsky, Lateral scan profiles of the recombination parameters correlated with distribution of grown-in impurities in HPHT diamond, Diamond and Related Materials. 47 (2014) 15–26.

31. C. Phaal, Plastic deformation of diamond, Philosophical Magazine 10 107 (1964) 887-891.

32. I.I. Vlasov, V.G. Ralchenko, E.D. Obraztsova, A.A. Smolin, V.I. Konov, Analysis of intrinsic stress distribution in grains of high quality CVD diamond film by micro-Raman spectroscopy, Thin Solid Films 308 (1997) 168-172.

33. I. Vlasov, V. Ralchenko, D. Zakharov, N. Zakharov, Intrinsic stress origin in high quality CVD diamond films, Physica status solidi (a) 174 1 (1999) 11-18.

34. M. Moore, M. Golshan, G. Kowalski, J. Reid, S. Collins, B. Murphy, Reciprocal-space mapping of synthetic and natural diamond, Journal of Physics D: Applied Physics, 32 (1999) A37.

35. J.B. Wu, M.L. Lin, X. Cong, H.N. Liu, P.H. Tan, Raman spectroscopy of graphene-based materials and its applications in related devices, Chemical Society Reviews 47 5 (2018) 1822-1873.

36. D. Kirillov, G.J. Reynolds, Linewidths of phonon lines of natural and synthetic diamonds, Applied physics letters 65 13 (1994) 1641-1643.

37. N.V. Surovtsev, I.N. Kupriyanov, V.K. Malinovsky, V.A. Gusev, Y.N. Pal'yanov, Effect of nitrogen impurities on the Raman line width in diamonds, Journal of Physics: Condensed Matter 11 24 (1999) 4767-4774.

38. T. Bauer, M. Schreck, H. Sternschulte, B. Stritzker, High growth rate homoepitaxial diamond deposition on off-axis substrates, Diamond and related materials 14 3-7 (2005) 266-271.

39. M. Muehle, M.K. Yaran, M.F. Becker, T. Schuelke, J. Asmussen, Y. Gu, D.K. Reinhard, T. A. Grotjohn. Quality and internal stress of single crystalline diamond synthesized by microwave plasma assisted chemical vapor deposition. In New Diamond and Nano Carbons Conference. 2012, May. Poster (available online at http://mipse.umich.edu/files/MIPSE_GS2012_Muehle2.pdf).

40. M.H. Grimsditch, E. Anastassakis, M. Cardona, Effect of uniaxial stress on the zone-center optical phonon of diamond, Physical Review B 18 2 (1978) 901.

41. J.W. Ager III, M.D. Drory, Quantitative measurement of residual biaxial stress by Raman spectroscopy in diamond grown on a Ti alloy by chemical vapor deposition, Physical Review B 48 4 (1993) 2601.

42. S. Prawer, R.J. Nemanich, Raman spectroscopy of diamond and doped diamond, Philosophical Transactions of the Royal Society of London, Series A: Mathematical, Physical and Engineering Sciences 362 1824 (2004) 2537-2565.

43. F. Ahmed, K. Durst, S. Rosiwal, J. Fandrey, J. Schaufler, M.Göken, In-situ tensile testing of crystalline diamond coatings using Raman spectroscopy, Surface and Coatings Technology 204 6-7 (2009) 1022-1025.

44. W.J.P. Van Enckevort, H.G.M. Lochs, Photoluminescence tomography as a method to image point-defect distributions in crystals: Nitrogen-vacancy pairs in synthetic diamonds, Journal of applied physics 64 1 (1988) 434-437.

45. A.M. Zaitsev, Optical Properties of Diamonds: a Data Handbook, Springer, Berlin, 2001.

46. Y. Nisida, Y. Mita, K. Mori, S. Okuda, S. Sato, S. Yazu, M. Okada, Color centers in annealing of neutron-irradiated type Ib and Ia diamonds, Materials Science Forum, 38-41 (1989) 561-566.

47. A.T. Collins, The characterization of point defects in diamond by luminescence spectroscopy. Diamond and related materials 1 5-6 (1992) 457-469.

48. E.J. Brookes, J.D. Comins, R.D. Daniel, R.M. Erasmus, A study of plastic deformation profiles of impressions in diamond, Diamond and related Materials 9 3-6 (2000) 1115-1119.

49. Y. Mita et al., Photochromism of H2 and H3 centres in synthetic type Ib diamonds, Journal of Physics: Condensed Matter 2 43 (1990) 8567.

50. S.C. Lawson et al., The 'H2' optical transition in diamond: the effects of uniaxial stress perturbations, temperature and isotopic substitution, Journal of Physics: Condensed Matter 4 13 (1992) 3439.

51. V.G. Vins, A.P. Yelisseyev, V. Sarin, Physics behind the modern methods of enhancement of natural diamonds, Precious Metals and Gem Stones 12 180 (2008) 155-163; ibid. 2 182 (2009) 132-145; ibid., 3 183 (2009) 127-148. (in Russian).

52. Y.V. Babich, B.N. Feigelson, I.Y. Babich, A.I. Chepurov, Specifics of the distribution of nitrogen defects in synthetic diamonds of cubic habit: IR mapping data, Geochemistry International 48 10 (2010) 1028-1034.

53. S.C. Lawson, H. Kanda An annealing study of nickel point defects in high-pressure synthetic diamond, Journal of applied physics 73 8 (1993) 3967-3973.

54. S.C. Lawson, H. Kanda, Nickel in diamond: an annealing study, Diamond and Related Materials 2 2-4 (1993) 130-135.

55. J.R. Kim, D.K. Kim, H. Zhu, R. Abbaschian, High pressure and high temperature annealing on nitrogen aggregation in lab-grown diamonds. Journal of materials science 46 19 (2011) 6264-6272.

56. T.A. Collins, P.M. Spear, The 1.40 eV and 2.56 eV centres in synthetic diamond, J. Phys. C: Solid State Phys 16 (1983) 963–973.

57. A.T. Collins, M. Stanley, Absorption and luminescence studies of synthetic diamond in which the nitrogen has been aggregated, J. Phys. D. Appl. Phys 18 (1985) 2537–2545.

58. A.T. Collins, Spectroscopic studies of synthetic diamonds grown by the temperature gradient method, Science and Technology of New Diamond, KTK Scientific Publishers, Tokyo Terra Scientific Publishing Company Tokyo (1990) 273-278.

59. E. Pereira, L. Santos, L. Pereira, D.M. Hofmann, P. Christmann, W. Stadler, B.K. Meyer, Slow emission of the 2.56 eV centre in synthetic diamond, DRM 4 (1994) 53–58.

60. M.N. Nazare, P.W. Mason, G.D. Watkins, H. Kanda, Optical detection of magnetic resonance of nitrogen and nickel in high-pressure synthetic diamond, Phys. Rev. B 51 (1995) 16741.

61. H. Kanda, X. Jia, Change of luminescence character of Ib diamonds with HPHT treatment, Diamond and related materials 10 9-10 (2001) 1665-1669.

62. A.T. Collins, S.H. Robertson, Cathodoluminescence studies of sintered diamond, Journal of materials science letters 4 6 (1985) 681-684.

63. R.C. DeVries, Plastic deformation and "work-hardening" of diamond, Materials Research Bulletin 10 11 (1975) 1193-1199.

64. D.J. Weidner, Y. Wang, M. T. Vaughan, Strength of diamond, Science, 266 5184 (1994) 419-422.

65. C.A. Brookes, V.R. Howes, A.R. Parry, Multiple slip in diamond due to a nominal contact pressure of 10 GPa at 1000° C, Nature 332 6160 (1988) 139-141.

66. M. Seal, Graphitization and plastic deformation of diamond, Nature 182 4645 (1958) 1264-1267.

67. T. Evans, S.T. Davey, S.H. Robertson, Photoluminescence studies of sintered diamond compacts, Journal of materials science, 19 7 (1984) 2405-2414.

68. E. Gaillou, J.E. Post, N.D. Bassim, A.M. Zaitsev, T. Rose, M.D. Fries, J.E. Butler, Spectroscopic and microscopic characterizations of color lamellae in natural pink diamonds. Diamond and Related Materials 19 10 (2010) 1207-1220.

69. A.T. Collins, Vacancy enhanced aggregation of nitrogen in diamond, Journal of Physics C: Solid State Physics 13 14 (1980) 2641.

70. R. Jones, J.P. Goss, H. Pinto, D.W. Palmer, Diffusion of nitrogen in diamond and the formation of A-centres. Diamond and Related Materials 53 (2015) 35-39.

71. O.G. Lysenko, V.I. Grushko, E.I. Mitskevich, G.D. Ilnitska, A.Yu. Boyarintsev, Yu.D. Onufriev, V.F. Popov, L.G. Levchuk, N.M. Kazuchits, M.S. Rusetsky, V.V. Lysakovskyi, S.A. Ivakhnenko, Luminescent and radiation characteristics of monocrystalline diamond powders, Journal of Superhard Materials 41 1 (2019) 17–23.

72. O.A. Shenderova, A.I. Shames, N.A. Nunn, M.D. Torelli, I. Vlasov, A. Zaitsev, Synthesis, properties, and applications of fluorescent diamond particles, Journal of Vacuum Science & Technology B, Nanotechnology and Microelectronics: Materials, Processing, Measurement, and Phenomena 37 3 (2019) 030802.

73. N. Nunn, N. Prabhakar, P. Reineck, V. Magidson, E. Kamiya, W.F. Heinz, O. Shenderova, Brilliant blue, green, yellow, and red fluorescent diamond particles: synthesis, characterization, and multiplex imaging demonstrations, Nanoscale 11 24 (2019) 11584-11595.